Optics and Lasers in Engineering 106 (2018) 147–154

Contents lists available at ScienceDirect

Optics and Lasers in Engineering

journal homepage: www.elsevier.com/locate/optlaseng

LCoS display phase self-calibration method based on diffractive lens schemes

Haolin Zhang[a,*], Angel Lizana[a], Claudio Iemmi[b], Freddy A. Monroy-Ramírez[c], Andrés Márquez[d], Ignacio Moreno[e], Juan Campos[a]

[a] Departamento de Física, Universitat Autònoma de Barcelona, Bellaterra, 08193, Spain
[b] Universidad de Buenos Aires, Facultad de Ciencias Exactas y Naturales, Departamento de Física, Consejo Nacional de Investigaciones Científicas y Técnicas, Buenos Aires, Argentina
[c] Departamento de Física, Universidad Nacional de Colombia - Sede Bogotá Carrera 45 No 26–85, Bogotá D.C. - Colombia
[d] Departamento de Física, Ingeniería de Sistemas y Teoría de la Señal, Universidad de Alicante, 03080, Alicante, Spain
[e] Departamento de Ciencia de Materiales, Óptica y Tecnología Electrónica, Universidad Miguel Hernández de Elche, 03202 Elche, Spain

ARTICLE INFO

Keywords:
Calibration
Liquid crystals
Optical metrology
Phase shifting interferometry
Surface measurement

ABSTRACT

An experimental method to calibrate Liquid Crystal on Silicon (LCoS) displays by self-generating lens configurations on the studied device is proposed in this paper. On the one hand, a split-lens is displayed in the LCoS to self-generate an interference pattern from which the phase-voltage curve of the modulator is calculated. On the other hand, a microlens array is displayed on the LCoS, within a same experimental set-up, to implement a Shack-Hartmann (S-H) wavefront sensor, from which the display surface profile is retrieved. Specifically, by means of a feasible set-up, the proposed method allows measuring the deviation from flatness of the LCoS displays as well as to determine the phase-voltage response of phase-only SLMs. Experimental results demonstrate a linear tendency phase-voltage curve that ranges from 0 rad up to ~6.28 rad, for the used light wavelength. Moreover, by extracting the LCoS phase distribution measured with the S-H configuration, the LCoS surface inhomogeneity is corrected by 95%.

1. Introduction

Liquid Crystal Display (LCD) is a mature technology widespread used in optical based applications. Thanks to their capability to spatially manipulate the phase properties of light beams, they are commonly used as Spatial Light Modulators (SLM) to manipulate the complex wavefront amplitude. For instance, they are applied in adaptive optics, to correct the wavefront aberration introduced by turbulence [1,2]; in metrology, to control phase distributions in interferometers [3,4]; in waveguide technology, to achieve wavelength selective switch systems, or to manipulate the lightwaves [5–7]. As the phase properties can be modified by controlling the voltages address to the SLM, LCDs are also commonly used in dynamic processes. For instance, for the generation of diffractive optical elements (DOEs) in diffractive optics applications [8,9]. They as well stand as important components in real-time laser beam shaping [10–12], and in structured illumination systems [13,14]. LCDs are also used to implement optical tweezers [15,16], digital lenses with improved performance [17,18], or optical encryption [19], etc.

Liquid Crystal on Silicon (LCoS) displays [20] are a class of LCD that work in reflective configuration. By selecting the proper input polarization [21], the LCoS performance can be optimized and we can select a phase-only or an amplitude-only regime. When using a phase-only configuration, the phase modulation can by digitally controlled by addressing a proper Diffractive Optical Element (DOE) to the LCoS. A number of improvements, such as high resolution, small pixel size, and very appealing fill factor (usually ~90%), are presented when comparing these reflective devices with transmissive LCDs. More importantly, LCoS displays present a larger phase modulation than transmissive devices with the same thickness, as light performs a double pass into the display.

Although the above-stated applications highlight the important role that LCoS play in different fields, to work with these devices in optimal conditions, efficient calibration and optimization of the spatial light modulators are required. As a consequence of the large demand of applications requiring the use of LCD technology, a widespread number of optimization methods can be found in literature [16,22–30], most of them based on interferometry [24–26] or diffraction [27,28]. Some authors have demonstrated that diffractive based methods, which may be valid for other LCDs, are not suitable to be applied with LCoS displays [23], mainly due to the time-fluctuations of the phase phenomenon (also referred as flicker effect). Under this scenario, alternative optimizing

* Corresponding author.
E-mail address: haolin.zhang@uab.cat (H. Zhang).

https://doi.org/10.1016/j.optlaseng.2018.02.019
Received 20 December 2017; Received in revised form 23 February 2018; Accepted 27 February 2018
0143-8166/

methods were proposed to take into account this effect [29–33] and different strategies have also been reported to minimize the observed DOEs efficiency loss associated to large phase-fluctuations [34,35].

Another critical drawback present in LCDs, both working in transmissive or reflective configurations, is related to inhomogeneities in the display flatness. These spatial inhomogeneites (which are related to different causes, such as screen lateral stresses or glass thickness variations), introduce an extra spatial phase distribution that degrades the performance of the modulator. Thus, this extra phase distribution must be taken into account for a proper calibration. As a consequence, different experimental strategies have been proposed to measure the display profile in order to compensate the screen inhomogeneities [16,36–38].

Recently, the idea of self-calibrating LCDs was proposed by J. L. Martinez et al. [31] by the means of addressing some DOEs on the LCD. The self-calibrating approach presents some advantages compared with standard calibrating methods. For instance, they avoid the necessity of using additional optical elements (i.e., without requiring external optical arrangements –as the commonly used interferometry, diffraction or polarization based set-ups). In fact, the same LCD to be calibrated is employed to display the optical element that allows the measurement. In Ref. [31], the overall averaged phase modulation of the device was evaluated by simultaneously addressing two diffractive elements displayed on two different halves of the LCoS. In one half, a uniform image or 'piston' was displayed. Then, different constant gray levels were added to this image so that this part acted as a phase-shifting mirror. In the other half of the screen, a symmetric binary phase grating was displayed. By selecting the proper diffractive order generated by the grating, this second half acted as a tilted reference plane-wave that interfered with the wave coming from the 'piston'. Note that different gray levels added to the piston led to different displacements of the interference pattern, from which the overall phase modulation of the device was determined. The method was also used to spatially resolve the phase-voltage curve. Nevertheless, this approach does not provide the deformation of the screen. As stated above, a complete description of the modulator also requires taking into account the screen deformation.

In this work we provide an alternative self-calibration method, based on addressing different diffractive lens configurations, valid to both characterize the overall phase-gray level performance and the screen profile of LCDs. In particular, the self-generation of two different diffractive-lens based DOEs is proposed. The first one consists of addressing a split-lens configuration [14], which leads to a simple direct implementation of an interferometric system, from which the overall phase distribution as a function of the addressed voltage is obtained. It is worth to mention that this method is valid even in presence of time-fluctuations of the phase [23], because it is able to give the required average phase as a function of the applied voltage. Furthermore, by addressing a second diffractive pattern, it is also possible to self-determine the screen profile of the display without any modifications of the optical set-up. This is achieved by properly addressing an arrangement of dynamic microlenses to the LCoS display (Shack-Hartmann wavefront sensor configuration [39,40]) and performing an iterative scanning process. We want to note that the propose method not only allows providing a complete calibration of the LCoS, by simply self-addressing different DOEs, but also determining these important characteristics just by using the same feasible and compact experimental set-up.

The outline of this work is as follows. In Section 2, we describe the proof of concept of the method used to self-calibrate the phase-voltage curve of the LCoS. Next, in Section 3, we describe the technique based on a Shack-Hatmann configuration, used to perform the self-measurement of the LCoS screen profile. In addition, the generation of the microlens array system and the ulterior retrieving of the screen profile, from the local light focalizations, are discussed. Afterwards, the methods described in Sections 2 and 3 are experimentally implemented and the corresponding results are shown and discussed in Section 4. Finally, the main conclusions of the work are provided in Section 5.

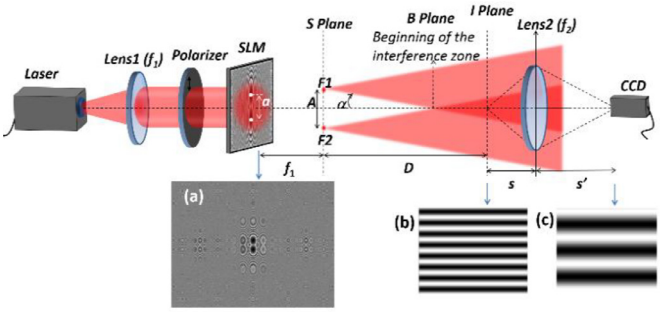

Fig. 1. Scheme of the optical set-up used to perform the phase-voltage calibration of the SLM.

2. LCoS phase-voltage self-calibration based on split lenses

In this section we describe a self-calibration method, based on split-lens configurations, to determine the phase-voltage curve of SLMs. This is an interferometic-based method, and thus, it is valid to be used even in presence of time-fluctuations of the phase [24], a non-desired phenomenon observed in some reflective LCoS displays.

The main idea consists of addressing a DOE to the LCoS in order to create a controlled interferometric pattern onto a propagated plane. In this way, the generated digital element replaces interferometric external set-ups commonly used to calibrate the phase-modulation of LCoS. In particular, we use as DOE the two-sectorial split-lens scheme described in Ref. [14]. This distribution is equivalent to the classical Billet lens configuration which consists of a lens split in two halves, and where the centers of those halves are transversally separated to a certain distance a. Under this scenario, each one of the two split-lens sectors leads to a focalization spot on the focal plane. These two light spots can be understood as two new coherent light sources that produce an interference fringe pattern onto a propagated plane. Although, in principle, this would be equivalent to the Young's experiment, in the Billet lens case the light passing through the separation between the two lens halves also adds a non-desired contribution in the interference pattern. This situation is solved by displaying a two-sectorial split lens onto a SLM, in a way that the corresponding phase distribution fully covers the modulator screen. Under this scenario, the composed diffractive lens gives place to two light spots at the focal plane, generating the interference fringes pattern at the far field [14]. What is more, some properties of the pattern can be digitally modified just by tuning few physical parameters of the system (e.g., the axial plane where the interference pattern is produced or the pattern period can be changed by tuning the focal length of the two split-lenses or the distance a between the halves centers, respectively).

A sketch of the optical set-up used to self-calibrate an SLM is shown in Fig. 1. A collimated polarized laser beam illuminates the SLM with the two-sector lens addressed on it, which give place to the generation of two focalization spots (F1 and F2 in Fig. 1) in the focal plane (S plane in Fig. 1). These two new light sources F1 and F2, with the same intensity, produce a fringes-like interference pattern in the far field. As it was previously pointed out, the properties of the split-lens (lens focal length, distance to the centers a, lens sectors orientation, etc.) are digitally controlled. An example of a particular phase distribution to be addressed to the SLM, corresponding to a lens split in two sectors vertically separated a distance a, can be seen in Fig. 1(a). As we are illuminating the SLM with a collimated beam, the two resulting sources F1 and F2 are separated a distance A equal to the selected distance a and to the same direction. This situation leads to horizontal fringes in a far field plane (e.g., I plane in Fig. 1). However, note that the direction of the fringes pattern could be controlled just by properly modifying the direction of separation between lens centers.

For the sake of clarity, the optical architecture in Fig. 1 is shown in a transmissive configuration. However, as it is explained in a forthcoming section, the real experimental implementation was performed in a reflective configuration because we analysed an LCoS display (reflective device). To adapt the scheme represented in Fig. 1 to the reflective configuration, a beam-splitter (B-S) was added in the optical arrangement.

As above-stated, by setting a distance a between the bi-lens centers (LCoS plane) and a focal length of f_1, two focused light spots with a separated vertical distance $A = a$ are generated at the focal plane (S plane) –see Fig. 1. Under this scenario, two spherical sources are created after the S plane, which can be understood as a new source plane. After being propagated to a certain distance, the two coherent beams are superposed and the corresponding fringes-shaped interference pattern is observed. In the scheme given in Fig. 1, the axial plane from which interference patterns begin to be observed is indicated with a dashed arrow (B Plane). Afterwards, a given interference pattern placed at a certain axial plane (I Plane; e.g., image (b) in Fig. 1) is selected. Finally, the interference pattern (image (c)) is imaged in the CCD camera with a certain magnification by using a convergent lens (Lens2 in Fig. 1). The use of Lens2 is not mandatory, but it is only introduced to obtain a more clear interference pattern at the CCD. Note that the angle α in Fig. 1 depends on both parameters a and f_1; thus, for a given axial plane, the distance between interference fringes (period) is tuned by using these two control parameters.

Once an interference pattern is recorded, the relation between the phase modulation and the gray level (voltage) addressed to the LCoS can be calibrated. To this aim, the phase distribution corresponding to one of the bi-lens sectors is not modified, but we gradually add a constant gray level to the other bi-lens sector. This scenario is achieved by the following phase-scheme to be addressed to the LCoS, which is inspired in the split-lens description given in Ref. [14],

$$U_{N=2}(r,\theta) = U_1 + U_2, \tag{1}$$

$$U_1 = \exp\left[i\frac{\pi}{\lambda f}\left(r^2 + {a_0}^2 - 2ra_0\cos(\theta_i - \theta_0)\right)\right], \tag{2}$$

$$U_2 = \exp\left[i\frac{\pi}{\lambda f}(r^2 + {a_1}^2 - 2ra_1\cos(\theta_{ii} - \theta_1) + \phi(V))\right], \tag{3}$$

where λ is the wavelength of the light source, f is the focal length and r is the radial coordinate in the plane of the lens; a_0 and a_1 are the distances of the two lens sector centers to the origin of coordinates, θ_0 and θ_1 are the angular positions of the two sector centers ($\theta_0 = \pi/2$ and $\theta_1 = 3\pi/2$ for the particular case shown in Fig. 1) and where θ_i and θ_{ii} are restricted into the ranges $[0, \pi)$ and $[\pi, 2\pi)$.

Note that in Eq. (3) there is a uniform (piston) phase value of ϕ, whose magnitude varies with the addressed voltage V. Therefore, each addressed voltage (gray level) will produce a change on the phase ϕ in the term U_2, which will yield a transversal shift in the fringes pattern. From those displacements, obtained for the whole available gray level range (0–255), the relation between the average phases versus addressed gray levels can be retrieved by using simple calculations, for instance, as done in Ref. [23].

3. LCoS flatness characterization based on micro-lens array (Shack–Hartmann distribution)

The screen of an ideal LCoS is homogeneous. However, mechanical stress and spatial defects generated during the fabrication of the LCoS displays always introduce certain amount of inhomogeneities to the screen. In order to achieve an optimal performance of these devices, the unwanted spatial phase distribution introduced by the screen should be compensated. To retrieve this spatial phase, we propose a second lens-based configuration that consists of a micro-lens array (Shark-Hartmann like sensor) able to self-calibrate the LCoS screen profile.

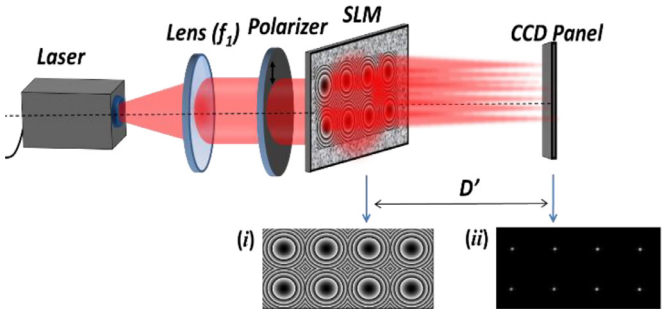

Fig. 2. Optical scheme used to self-calibrate the screen profile of LCoS. Inset images: (*i*) Phase distribution sent to the LCoS to generate a microlens array (Shack-Hartmann configuration); and (*ii*) Corresponding intensity distribution at the focal plane.

Shack-Hartmann (S-H) wavefront sensors have become a prevalent tool in many fields [39–41] because of their great capability to measure wavefront aberrations and their ability to provide an accurate wavefront map. In particular, each microlens focuses a fraction of the input wavefront onto the focal plane of the microlens array. If the input wave presents some spatial aberrations, the light spots are displaced from their expected ideal centers. By measuring such local deviations, and properly applying some numerical methods, the profile of the input wave can be retrieved.

The idea behind the proposed approach is to use the same LCD to be characterized to display the microlenses required in the S-H approach. The microlens array is perpendicularly illuminated with the collimated incident beam free of aberrations. Under this situation, in the presence of aberrations in the LCoS screen, the light spots generated by the microlenses deviate from their ideal positions, and those deviations are mainly related to the screen defects. Note that the LCoS screen self-calibration can be performed just by introducing the phase distribution corresponding to the S-H microlens array [39], and without modifications on the experimental set-up proposed in Section 2 (see Fig. 1). In particular, the optical scheme used for the LCoS screen self-calibration is sketched in Fig. 2.

In order to obtain the light spots pattern, a 4×2 microlenses configuration is generated onto the LCoS (LCoS plane in Fig. 2). The corresponding light spots distribution is obtained at the diffractive lenses focal plane. As an example, we show the phase distribution addressed to the LCoS to generate a 4×2 lens array and its corresponding light spots distribution at the CCD plane (inset images (*i*) and (*ii*), respectively). In our case, the dimension in pixels of the region selected to generate a single microlens was of 400×400 pixels, and thus, the whole set of 4×2 microlenses had a dimension of 1600×800 pixels.

It is important to note that the generated 4×2 microlens array does not cover the full pixel distribution of the modulator used in the experimental implementation (a PLUTO LCoS display; 1920×1080 pixels). On one side, we are interested in using microlens apertures as larger as possible, because this enhances the efficiency of the generated DOEs. However, a reduced number of microlenses implies that the spatial sampling of the screen is very low (in this case, only 8 sections of the screen are inspected). To solve this problem, a number of displacements of the whole 4×2 array was performed along the full screen. In particular, we performed 8 displacements of the array with a shift step of 50 pixels in both x and y directions. By combining that set of intensity patterns, a final image containing 512 bright intensity spots was constructed (see corresponding light spot pattern at Fig. 3(a)). From this final image, the full screen of the modulator can be studied with larger spatial resolution. For the sake of clarity, a video file recording the full scanning process is also provided (Video 1). Note that the microlens array scanning velocity in Video 1 was arbitrarily selected. If faster measurements are required, a higher velocity can be obtained by the user – the scanning velocity

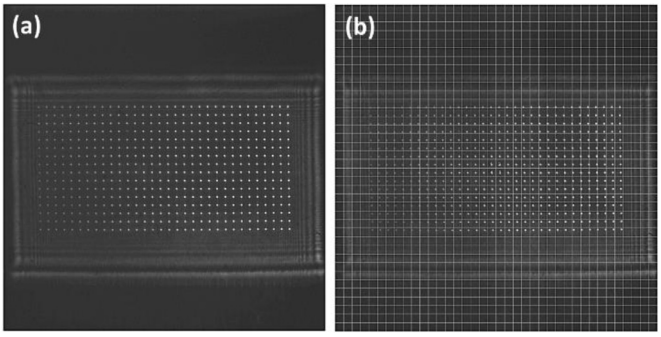

Fig. 3. (a) Light spot pattern at the CCD after scanning the full LCoS screen by using 8 displacements of the 4×2 lens array in both x and y directions (see Video 1); and (b) Same light-spot pattern combined with an over-imposed 38×38 square grid.

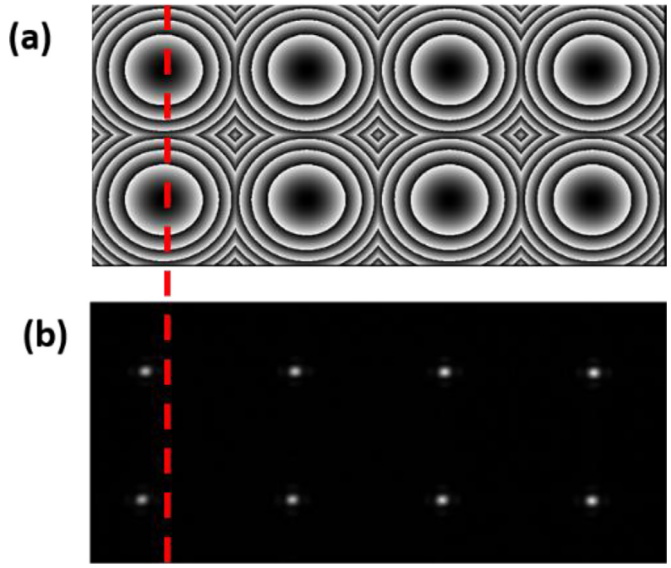

Fig. 4. (a) Phase distribution sent to the LCoS display to generate the 4×2 microlens array; and (b) Corresponding intensity distribution at the focal plane.

is limited by the refresh rate of the LCoS display (60 Hz in our case). Finally, if a different spatial resolution than that obtained in Fig. 3(a) and Video 1 is required, a different microlens array shift step could be easily selected as well.

Once the complete spot-light distribution is obtained, the LCoS shape can be retrieved from the deviation of each individual spot from its corresponding theoretical center. An example is shown in Fig. 4(a) and (b) for the particular case of 4×2 microlenses, where deviations between the centers of the microlenses generated at the LCoS and the recorded light spots are highlighted by the red-dashed line. The stated light-spot displacements were estimated by using centroid calculations, which were conducted based on a numerical algorithm inspired in that detailed in Ref. [40]. To accurately apply this algorithm, it is necessary to estimate the deviations of the measured light dots distribution at the CCD plane with respect to the theoretical centers (microlens array centers). To this aim, we used as theoretical-centers reference, a squared grid (38×38 squares in our case; see Fig. 3(b)). The deviations of the light-dots from the square centers are the values to be obtained.

At this point, it is worthy to discuss how to lay the reference-grid at the CCD plane to a proper usage. The ideal alignment of the grid is found when perfectly overlapping the squared grid centers with the projection of the microlens centers at the CCD plane, for the case of a wavefront free of distortions. Unfortunately, in the framework of our experimental set-up, this ideal-wavefront cannot be ever implemented to calibrate the grid position, because of the LCoS screen aberrations that always distort the input wavefront. This means that the light-dots are always deviated from their theoretical centers and we cannot use a reference light-dots distribution to center the grid.

Under this scenario, as the grid-coordinate origin is not known, we first arbitrary placed the grid at the CCD plane in such a way that the 2×2 central light dots of the full 32×16 pattern are centered as better as possible. This arbitrary selection of the grid origin has a potential problem that has to be discussed: a possible *x-y* displacement of the grid from the theoretical position. This situation leads to centroid calculations with added constant values. It is worthwhile remembering that light-dots deviations are related to LCoS profile derivatives. Thus, numerical integration has to be applied to retrieve the LCoS screen profile. In this context, constant values added at the dots-deviations lead to linear phases added at the final screen profile. This is not a significant problem because linear phases do not vary the characterization of the screen shape, but only introduce an artificial tilt which can be numerically extracted.

Moreover, another problem can arise from the grid selection, in particular if we select a square size different from the theoretical one. This situation has a major impact on the final LCoS profile calculation. In fact, if the grid square size differs from the actual one, linear phases are introduced in the centroids calculation. Hence, artificial quadratic errors are added to the screen profile after numerical integration. Under this scenario, to avoid these quadratic errors, which critically affect the final profile calculation, the grid square size cannot be arbitrarily selected but an accurate estimation is required. In our case, by considering a microlens-shift step of 50 pixels and the LCoS pixel size of 8 μm, the distance between the centers of two contiguous microlenses generated at the LCoS was of $50\times8=400$ (pixels·μm). Moreover, the resolution of the CCD (PCO.2000) was of 2048×2048 with a pixel size of 7.4 μm. Under this condition, we calculated the distance between two centers of the grid in the CCD, this value being the optimal square grid size (400 (pixels·μm) / 7.4 (μm)) = 54.05 pixels. According to this grid size, the number of the squares that fits in our CCD is of 37.9×37.9 (2048 pixels / 54.05 pixels). Hence, a 38×38 grid was implemented for the analysis of the obtained spot array. At this point, by considering the proper square size, the non-desired quadratic profile is minimized.

By following this approach, accurate spots displacements from the actual centers are obtained. Those displacements are related with local derivatives of the display profile, and thus, integration methods lead to a discrete function of the screen profile. Once this data is obtained, a cubic spline interpolation approach provides a continuous estimation of LCoS screen profile. The obtained experimental results are discussed in a forthcoming section (Section 4).

Last but not least, we want to emphasize that local variations of the average phase-voltage look-up table discussed in Section 2, may affect the efficiency of the generated microlens array, but do not affect the position of the lens focalizations, as those are only related with the screen profile. Thus, the method proposed to evaluate the aberrations introduced by LCoS displays is not affected by this spatial dependence of phase-voltage relation.

4. Experimental implementation of the methods

The phase-voltage calibration (Section 2) and the LCoS flatness (Section 3) methods rely on the same optical set-up. The SLM role described in Section 2 is conducted by an LCoS display in the experimental implementation. In fact, to change from one method to the other one, we only need to select the proper phase distribution to be addressed to the LCoS (split-lens or microlens array (S-H) configurations).

To experimentally test the validity of our proposed methods, the above-discussed optical layout was experimental implemented. Fig. 5 shows a photograph of the implemented experimental set-up from two different points of view (Fig. 5(a) and (b), respectively) and a detail of the used LCoS (Fig. 5(c)). A polarized He-Ne laser (632.8 nm) was cho-

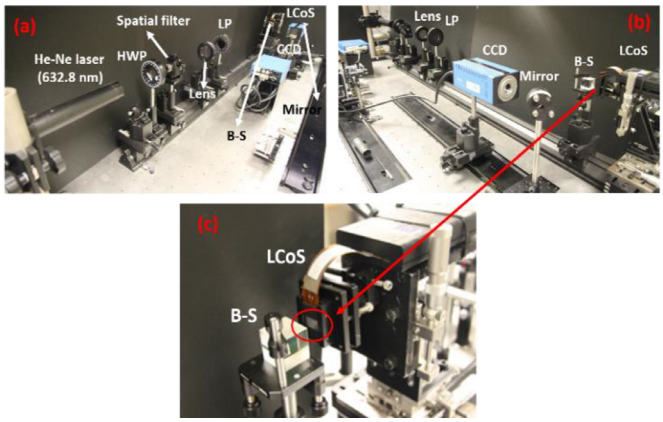

Fig. 5. Experimental set-up used for the LCoS characterization: (a) Experimental set-up from the laser source point of view; (b) Experimental set-up view from the LCoS; and (c) Detail of the reflective screen of the LCoS under calibration.

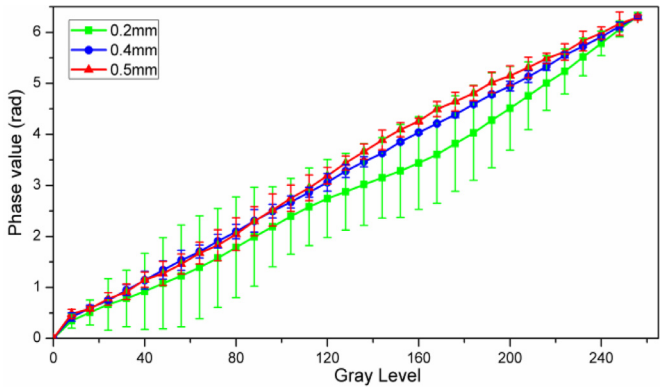

Fig. 6. Average phase modulation (in rad) versus addressed gray level measured using two split lens sectors with center separations of 0.2 mm, 0.4 mm and 0.5 mm.

sen as a light source. Afterwards, a combination of a Spatial Filter, including a microscope objective (×20), a pinhole, and a convergent lens with $f = 200$ mm, were used to generate a collimated and filtered light beam. Note that for successfully applying the shape-calibration method described in Section 3, an input beam as close as possible to a collimated beam is required to mimic a plane wave free of aberrations. In this way, all the spatial aberrations of the reflected wave are only associated to the LCoS. If the input light is not perfectly flat, the spot array locations at the focal plane are not only influenced by the LCoS display deformation but also by the effect of the unideal input wavefront profile. Under this scenario, the final reconstructed surface profile accounts for the overall wavefront deformation. If the final purpose is to correct the effect of the LCoS display for any applications (the introduction of the extra phase distribution related to the display inhomogeneity), the input wavefront shape is not so crucial, because our self-calibrating method will allow us to both correct the LCoS display deformation and the optical system misalignments (the overall wavefront deformation). However, if the main aim is to measure the specific LCoS display surface profile, a precise alignment is mandatory and the quality of the input collimated beam needs to be evaluated (we require an input wavefront as flat as possible). To provide this last situation, we used a shearing interferometer (SI050 shear-plate, distributed by Thorlabs) to conduct qualitative analysis of the flatness and the collimation of the input beam. The measurements provided by the shearing interferometer demonstrated an ideal collimated light (into the device precision), revealing that the setup was well aligned.

Afterwards, the intensity of light illuminating the LCoS was controlled by properly orienting the relative angle between a half-waveplate and a linear polarizer (HWP and LP in Fig. 5), both of them are distributed by Meadowlark Optics. In addition, the LP was oriented in a way that optimized the pure phase modulation provided by the LCoS (parallel to the liquid crystal director orientation). We used a PLUTO parallel aligned LCoS distributed by HOLOEYE. This is an active matrix reflective device with 1920 × 1080 resolution and with a pixel size of 8 μm. The display has a fill factor of 87%, a reflectivity of 65–70%, and diffraction efficiency of more than 80%.

As LCoS displays are reflective devices, a beam-splitter (B-S in Fig. 5) was placed before the LCoS in order to set 90° between the incident and the reflected beam. Afterwards, a mirror steers the reflected beam to the backward direction. In this work, the DOEs addressed to the LCoS are those explained in Sections 2 and 3. In the S-H configuration case (see Section 3), a CCD camera was placed at the micro-lens focal plane, where the corresponding light-spots array was imaged. In the case of the split-lens configurations (see Section 2), the axial plane of interest is that where interferences take place. As the CCD camera, we used a PCO.2000 camera with a resolution of 2048 × 2048 pixels.

Once the set-up was implemented, the two self-calibration methods were experimentally tested, as provided in the following Sections 4.1 and 4.2, for obtaining the phase-voltage look-up table and the LCoS aberration evaluation, respectively.

4.1. Average phase versus voltage self-calibration test

A split-lens configuration with two sectors, as that described in Section 2 (see Fig. 1), was addressed to the LCoS. The sectors were set with a focal length of 350 mm and a distance separation a_0-a_1 between the split-lens centers of 0.2 mm. This phase pattern was progressively modified by adding a constant gray level (related to the parameter $\phi(V)$ in Eqs. (1) and (3)) to the second split lens (the one below in Fig. 1) from 0 to 255 in steps of 8. Under this scenario, 33 intensity patterns (interference fringes) were captured with the CCD camera (one pattern for each added constant value $\phi(V_i)$). Note that each new constant phase leads to a fringe pattern displaced to a certain value in the horizontal direction. Once this set of 33 interference patterns was grabbed, a post-processing was conducted. We performed cross-correlations ($C_{V0,Vi}$) between a reference pattern (interference pattern for the gray level 0; V0) and the rest of the interference patterns (related to different gray levels; V*i*). The distance between the maximum of the self-correlation $C_{V0,V0}$ and the cross-correlations $C_{V0,Vi}$ gave us the shift of each particular fringe pattern with the applied gray level. These distances are directly related to the phase modulation, so the experimental phase-voltage characteristic curve of the LCoS display was obtained. As the integration time of the CCD (~0.5 s) was set longer than the typical period of the LCoS flickering (~8 ms [23,32–34]) the proposed calibration method provides mean phase values resulting from the average of the phase fluctuations. But this, far from being a problem is an advantage, since these mean values are the adequate conditions to optimize the efficient generation of DOEs [23].

In order to study the robustness of the method, the mean-phase value corresponding to each addressed gray level was measured one hundred times and the corresponding standard deviations were calculated. The derived average phase values as a function of the addressed gray level are represented in Fig. 6 (green squares) and the corresponding standard deviations are given as error bars in the graphic. The same experiment was repeated for two extra separations between the split-lens centers. In particular, blue-circles and red-triangles in Fig. 6 correspond to 0.4 mm and 0.5 mm split-lens center distances, respectively.

We see how the three curves in Fig. 6 give similar results in terms of the mean phase values, all of them showing a phase variation from 0 rad up to ~6.28 rad with a linear tendency, this being in agreement with the commercial specifications for the used light wavelength. More-

over, the green curve is the one showing the largest discrepancies with the other two curves. To determine which curve better describes the real phase modulation of the LCoS, we take into account the associated standard deviations. In fact, we observe how the robustness of the method strongly depends of the split-lens distance selected. In this sense, error bars associated to the green curve (0.2 mm distance between the split-lens) are very large (a maximum error of 0.98 rad), whereas the blue and the red curves (0.4 mm and 0.5 mm cases, respectively) lead to much smaller errors, the smallest one corresponds to 0.4 mm case (maximum error of 0.22 rad). This fact can be related with the above-described correlation process underneath the phase calculations, which becomes more efficient for a proper number of fringes at the CCD camera. In this sense, different split-lens center distances lead to different interference fringe periods at the CCD camera. Thus, before using the self-calibration method to retrieve the phase-voltage curve of LCoS displays, to set the optimal fringes period (i.e., split-lens distance) at the CCD camera is recommended. In our case, the best result, in terms of associated data errors, is obtained for a split-lens distance of 0.4 mm (blue data in Fig. 6).

4.2. LCoS display spatial shape characterization test

In this final section we focus on the experimental results obtained when experimentally applying the method described in Section 3 for the LCoS flatness characterization. To this aim, the same above-described experimental set-up is used (see Fig. 5). As explained before, a 4×2 microlens array was displayed on a region of the LCoS and then it was displaced along the LCoS screen both in the x and y directions with controlled shifts (50 pixels). Each location of the 4×2 microlens array generated a 4×2 spot pattern on the CCD camera (see inset images (*i*) and (*ii*) in Fig. 2). The combination of all these images led to a final pattern consisting of 32×16 light-spots, see Fig. 3(a). The spatial resolution of the technique depends on the microlens array displacement step chosen and the LCoS pixel size (8 μm in our case). By calculating the distances of those light spots to their theoretical centers, according to centroid calculations [28] (see Section 3), the local derivatives were retrieved. From those derivatives values, the LCoS screen flatness was calculated by properly applying integration methods. Finally, a continuous function of the LCoS aberrations was obtained by using a cubic spline interpolation, as explained in Section 3.

The obtained results when scanning the LCoS display in Fig. 5 are shown in Fig. 7(a), where it is observed a quadratic aberration that is typically related with lateral mechanical stress applied at the edges of the screen during fabrication. For the sake of clarity, the retrieved LCoS screen phase distribution is represented in modulus 2π in Fig. 7(b).

To test the validity of the obtained result, a further experiment was performed. In particular, we checked the correctness of the phase distribution shown in Fig. 7 by using it to compensate the LCoS screen aberration. In particular, by addressing the inverse of the phase-function in Fig. 7(a) to the LCoS display, the screen aberration should be compensated and each light spot of the final 32×16 distribution should fall into its corresponding theoretical center. This was experimentally performed, and the corresponding compensated LCoS screen profile was measured by using once again the S-H method. The obtained compensated spatial profile is given in Fig. 8(a). As complementary representation, the LCoS screen phase distribution is plotted in modulus 2π in Fig. 8(b).

Note that the compensated LCoS phase distribution (Fig. 8(a)) presents a significantly smoother profile compared to that represented in Fig. 7(a) since the quadratic aberration was almost removed. Note that the worst screen profile estimation is found at the image edges (corner regions in Fig. 8(a)). This is due to the lack of overlapping information in such regions during the scanning process (see Video 1). Accordingly, the aberration function at the edges is obtained by using extrapolation methods while the rest of the aberration function is more accurate because it is determined through cubic spline interpolation. Note that while sev-

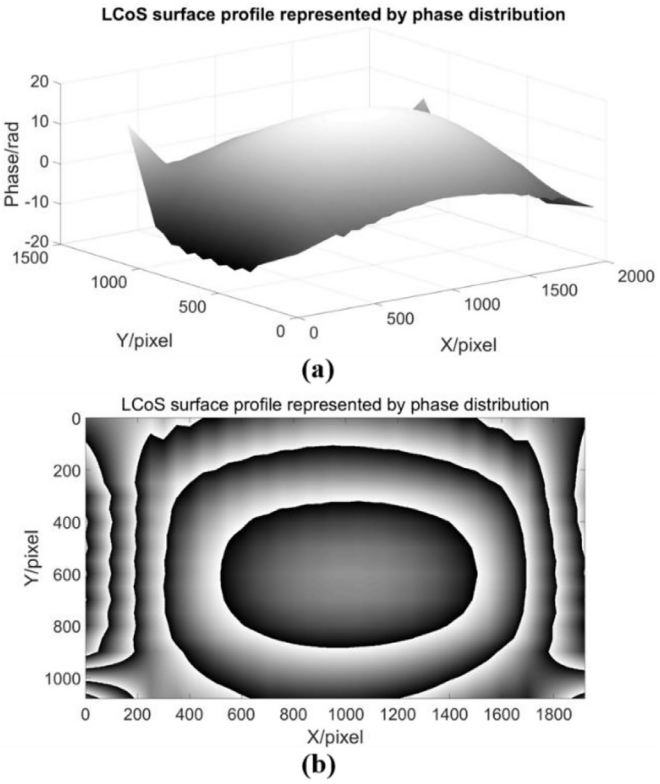

Fig. 7. (a) LCoS screen surface profile retrieved by using the S-H based method; and (b) LCoS display phase distribution (modulus of 2π).

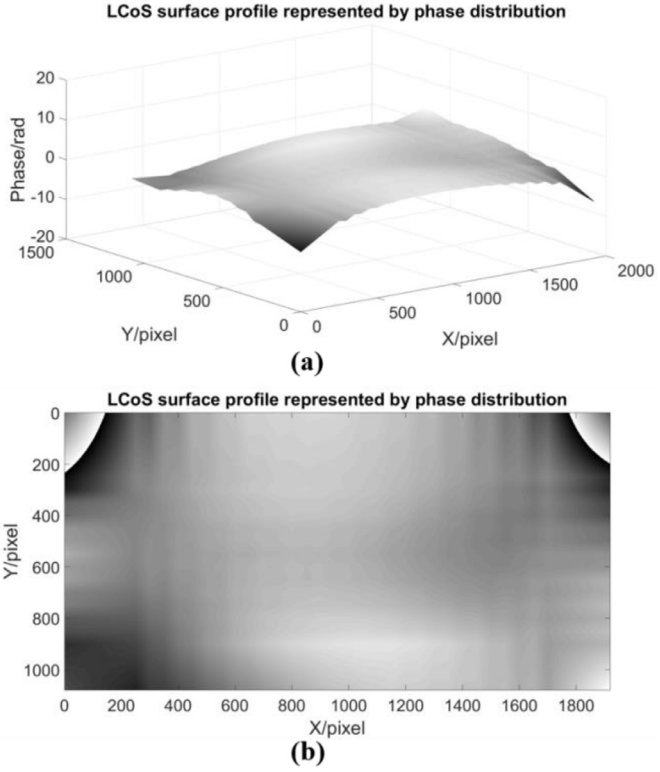

Fig. 8. (a) Compensated LCoS screen surface profile retrieved by introducing the inverse of the phase distribution in Fig. 7(a); and (b) Corrected phase distribution of the LCoS display (modulus of 2π).

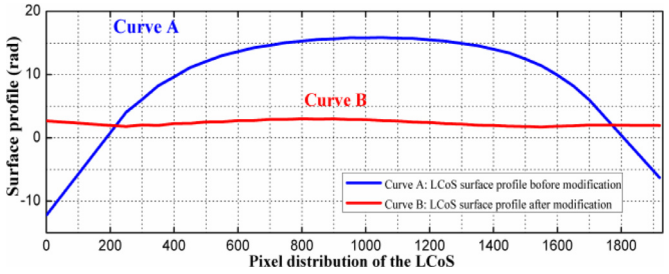

Fig. 9. LCoS surface phase values for a horizontal line: (a) The original LCoS surface profile before modification; and (b) The LCoS surface profile after correction.

eral 2π phase jumps are presented in Fig. 7(b), phase values in Fig. 8(b) are restricted in a significantly reduced phase range, this pointing out the improvement of the LCoS screen flatness.

To better quantify the capability of the method to correct the LCoS aberration, we compare the phase values along a horizontal line both in Figs. 7(a) and 8(a) (from the middle pixel of the left edge to the middle pixel of the right edge). Obtained results are given in Fig. 9 for the original LCoS flatness (blue curve A) and the compensated LCoS flatness (red curve B). The successful application of the method is clearly demonstrated by directly comparing the blue and red curves in Fig. 9. Whereas the LCoS screen profile in the chosen direction follows a quadratic function (Curve A in Fig. 9), the corrected profile is almost flat (curve B). In particular, the obtained maximum phase value and the minimum phase value in the original retrieved profile are of 15.85 radians and −12.16 radians, presenting a peak-to-valley (PV) surface profile error of 28.01 radians. The maximum and the minimum phase values in the corrected profile are of 3.02 radians and 1.74 radians, providing a surface profile PV error of 1.28 radians. The above-mentioned results demonstrate an efficient correction of the aberration in the LCoS display by providing a 95% surface flatness improvement.

5. Conclusion

In summary, we present an experimental method based on the generation of diffractive lens configurations for the optical characterization of Liquid Crystal on Silicon (LCoS) displays. The novelty of this method resides on applying different self-calibrating patterns (diffractive lenses schemes) to determine both the LCoS phase-voltage look-up table and its surface profile, without the necessity of using external optical arrangements (as usually happens by using interference or diffractive based calibration set-ups). The self-calibration configuration is set by self-addressing the calibrating DOEs to the LCoS under measurement. More importantly, compared to common LCoS calibration methods, which measure the surface profile and the phase-voltage curves by using two distinctive experimental set-ups, our method allows retrieving these two important LCoS characteristics with a single experimental scheme.

In particular, two optical diffractive lens-based schemes are proposed: a two sectors split-lens configuration and a micro-lens array (Shack-Hartmann) configuration. The first method (split-lens configuration) allows generating a controlled interference pattern, equivalent to the Young's experiment, resulting from the controlled interference of two self-generated plane-waves propagating with different wave-vectors. The particular wave-vectors are customized by easily changing the distance between generated split-lens centers. By adding different gray-levels to one of the two propagating beams, the corresponding interference fringes pattern is shifted. From those displacements, the average phase-voltage look-up table of the examined LCD can be easily calibrated. Note that as the calibrating method is based on an interference scheme, this method is valid to provide the phase-modulation curve of LCDs even in presence of significant time-fluctuations of the phase [14]. The second method (micro-lens array) allows generating a light-spot distribution at the focal plane, containing information of the LCoS flatness. By spatially shifting the lens scheme addressed on the studied LCoS, the full screen area is scanned.

The method was experimentally validated by studying a particular LCoS display. The two-above stated schemes were experimentally implemented and the obtained results were discussed. We studied the influence of some split-lens control parameters in the resulting phase-voltage curve error, this allowing us to tune those parameters to obtain an optimal configuration. In addition, the experimental LCoS profile was also determined. From this obtained information, the validity of the method was tested by experimentally correcting the LCoS aberrations. Experimental results demonstrate a linear phase-voltage response of the calibrated LCoS, ranging from 0 rad up to ~6.28 rad. Moreover, the LCoS screen measurement showed a quadratic profile. By using our method, this screen aberration was corrected by 95%. The experimental results obtained, and the feasibility of the proposed technique, guarantee the potential of the optical method to be applied for LCoS displays calibration process.

Funding

H. Zhang acknowledges the financial support of the Chinese Scholarship Council (CSC) (No. 201504910783). H. Zhang, A. Lizana and J. Campos acknowledge the financial support of Spanish MINECO (FIS2015-66328-C3-1-R and fondos FEDER); Catalan Government (SGR 2014-1639). C. Iemmi acknowledges the financial support of UBACyT20020130100727BA, CONICET PIP 11220150100475CO, and ANPCYT PICT 2014/2432. Supplementary material associated with this article can be found, in the online version, at doi:10.1016/j.optlaseng.2018.02.019.

References

[1] Mu Q, Cao Z, Hu L, Li D, Xuan L. Adaptive optics imaging system based on a high resolution liquid crystal on silicon device. Opt Express 2006;14(18):8013–18.
[2] Wang C, Hu L, Yu H, Wang Y, Li D, Wang S, Mu Q, Yang C, Cao Z, Lu X, Xuan L. Wavefront detection method of a single-sensor based adaptive optics system. Opt Express 2015;23(16):21403–13.
[3] Twientmeyer KM, Chipman RA, Elsner AE, Zhao Y, VanNasdale D. Mueller matrix retinal imager with optimized polarization conditions. Opt Express 2008;16(26):21339–54.
[4] Soden RAJ, Dewhurst RJ. An integrated liquid crystal phase modulator for speckle shearing interferometry. Opt Lasers Eng 1999;31(2):123–34.
[5] Yang H, Robertson B, Yu D, Zhang Z, Chu DP. Origin of transient crosstalk and its resolution reduction in phase-only LCoS wavelength selective switches. J Lightwave Technol 2013;31(22):3822–9.
[6] Robertson B, Yang H, Redmond MM, Collings N, Moore JR, Liu J, Jeziorska-Chapman AM, Pivnenko M, Lee S, Wonfor A, White IH, Crossland WA, Chu DP. Demonstration of multi-casting in a 1×9 LCoS wavelength selective switch. J Lightwave Technol 2014;32(3):402–10.
[7] Suzuki K, Seno K, Ikuma Y. Application of waveguide/free-space optics hybrid to ROADM device. J Lightwave Technol 2017;35(4):596–606.
[8] Carles G, Muyo G, Bosch S, Harvey AR. Use of a spatial light modulator as an adaptable phase mask for wavefront coding. J Mod Opt 2010;57(10):893–900.
[9] Márquez JL, Fernández EJ, Prieto PM, Artal P. Chromatic aberration control with liquid crystal spatial phase modulators. Opt Express 2017;25(9) 9793-01.
[10] Rodrigo J, Alieva T, Abramochkin E, Castro I. Shaping of light beams along curves in three dimensions. Opt Express 2013;21(18):20544–55.
[11] Rodrigo J, Alieva T. Freestyle 3D laser traps: tools for studying light-driven particle dynamics and beyond. Optica 2015;2(9):812–15.
[12] Tong Z, Chen X. A ferroelectric liquid crystal spatial modulator encoded with orthogonal arrays and its optimized design for laser speckle reduction. Opt Lasers Eng 2017;90:173–8.
[13] Zheng X, Lizana A, Peinado A, Ramírez C, Martínez JL, Márquez A, Moreno I, Campos J. Compact LCoS–SLM based polarization pattern beam generator. J Lightwave Technol 2015;33(10):2047–55.
[14] Lizana A, Vargas A, Turpin A, Ramírez C, Estevez I, Campos J. Shaping light with split lens configurations. J Opt 2016;18(10):105605.
[15] Martín-Badosa E, Montes-Usategui M, Carnicer A, Andilla J, Pleguezuelos E, Juvells I. Design strategies for optimizing holographic optical tweezers set-ups. J Opt A-Pure Appl Opt 2007;9(8):S267.
[16] Bowman RW, Wright AJ, Padgett MJ. An SLM-based Shack-Hartmann wavefront sensor for aberration correction in optical tweezers. J Opt 2010;12(12):124004.
[17] Campos J, López-Coronado O, Iemmi C, Escalera JC, Gimeno R, Yzuel MJ. Multiplexed lenses written onto a liquid crystal display to increase depth of focus. In: Proc. SPIE, 6311; 2006. p. 63110Q.

[18] Márquez A, Iemmi C, Campos J, Escalera JC, Izuel MJ. Programmable apodizer to compensate chromatic aberration effects using a liquid crystal light modulator. Opt Express 2005;13(3):716–30.
[19] Tu H, Cheng C, Chen M. Optical image encryption based on polarization encoding by liquid crystal spatial light modulators. J Opt A-Pure Appl Opt 2004;6(6):524.
[20] Zhang Z, You Z, Chu D. Fundamentals of phase-only liquid crystal on silicon (LCoS) devices. Light Sci Appl 2014;3(10):e213.
[21] Moreno I, Lizana A, Campos J, Márquez A, Iemmi C, Yzuel M. J. Mueller-Stokes characterization and optimization of liquid crystal on silicon display showing depolarization. Opt Express 2008;16(3):1669–85.
[22] Yang L, Xia J, Chang CL, Yang ZM, Chen JH. Nonlinear dynamic phase response calibration by digital holographic microscopy. Appl Opt 2015;54(25):7799-7706.
[23] Lizana A, Moreno I, Márquez A, Iemmi C, Fernandez E, Campos J, Yzuel MJ. Time fluctuations of the phase modulation in a liquid crystal on silicon display: characterization and effects in diffractive optics. Opt Express 2008;26(21):16711–22.
[24] Ramirez C, Karakus B, Lizana A, Campos J. Polarimetric method for liquid crystal displays characterization in presence of phase fluctuations. Opt Express 2013;21(3):3182–92.
[25] Soutar C, Monroe SE, Knopp J. Measurement of the transmittance of the Epson liquid crystal television. Opt Eng 1994;33(4):1061–9.
[26] Bergeron A, Gauvin J, Gagnon F, Gingras D, Arsenault HH, Doucet M. Phase calibration and applications of a liquid crystal spatial light modulator. Appl Opt 1995;34(23):5133–9.
[27] Engström D, Milewski G, Bengtsson J, Galt S. Diffraction-based determination of the phase modulation for general spatial light modulators. Appl Opt 2006;45(28):7195-7104.
[28] Zhang Z, Lu G, Francis TS. Simple method for measuring phase modulation in liquid crystal televisions. Opt Eng 1994;33(9):3018–22.
[29] Martínez FJ, Márquez A, Gallego S, Francés J, Pascual I, Beléndez A. Retardance and flicker modeling and characterization of electro-optic linear retarders by averaged Stokes polarimetry. Opt Lett 2014;39(4):1011–14.
[30] Martínez FJ, Márquez A, Gallego S, Ortuño M, Francés J, Beléndez A, Pascual I. Averaged Stokes polarimetry applied to evaluate retardance and flicker in PA-LCoS devices. Opt Express 2014;22(12):15064–74.
[31] Martínez JL, Fernández EJ, Prieto PM, Artal P. Interferometric method for phase calibration in liquid crystal spatial light modulator using a self-generated diffraction-grating. Opt Express 2017;24(13):14159–71.
[32] Márquez A, Moreno I, Iemmi C, Lizana A, Campos J, Yzuel MJ. Mueller-Stokes characterization and optimization of a liquid crystal on silicon display showing depolarization. Opt Express 2008;16(3):1669–85.
[33] Lizana A, Moreno I, Iemmi C, Márquez A, Campos J, Yzuel MJ. Time-resolved Mueller matrix analysis of a liquid crystal on silicon display. Appl Opt 2008;47(23):4267–74.
[34] Lizana A, Márquez A, Lobato L, Rodagne Y, Moreno I, Iemmi C, Campos J. The minimum Euclidean distance principle applied to improve the modulation diffraction efficiency in digitally controlled spatial light modulators. Opt Express 2010;18(10):10581–93.
[35] García-Márquez J, López V, González-Vega A, Noé E. Flicker minimization in an LCoS spatial light modulator. Opt Express 2012;20(8):8431–41.
[36] Lopez-Quesada C, Andilla J, Martin-Badosa E. Correction of aberration in holographic optical tweezers using a Shack-Hartmann sensor. Appl Opt 2009;48(6):1084–90.
[37] Vargas J, Uribe-Patarroyo N, Quiroga JA, Alvarez-Herrero A, Belenguer T. Optical inspection of liquid crystal variable retarder inhomogeneities. Appl Opt 2010;49(4):568–74.
[38] Yun Z, Liu J, He Z, Li Y. Measurement of the thickness uniformity of liquid crystal layer. Appl Opt 1997;36(34):9109–10.
[39] Lobato L, Márquez A, Lizana A, Moreno I, Campos J. Characterization of a parallel aligned liquid crystal on silicon and its application on a Shack-Hartmann sensor. In: Proc. SPIE, 7797; 2010 77970Q-1.
[40] Schiegerling J, Dehoog E. Problems testing diffractive intraocular lenses with Shack--Hartmann sensors. Appl Opt 2008;47(25):4548–54.
[41] Smith DG, Greivenkamp JE. Generalized method for sorting Shack-Hartmann spot patterns using local similarity. Appl Opt 2010;49(16):D62–8.